Woven-Yarn Thermoelectric Textiles

Jae Ah Lee, Ali E. Aliev, Julia S. Bykova, Mônica Jung de Andrade, Daeyoung Kim, Hyeon Jun Sim, Xavier Lepró, Anvar A. Zakhidov, Jeong-Bong Lee, Geoffrey M. Spinks, Siegmar Roth, Seon Jeong Kim, and Ray H. Baughman**

Flexible, lightweight, textile-based thermoelectric (TE) generators are needed for powering electronic devices[1–4] and for harvesting electrical energy from the thermal energy of combustion engines and plant waste streams. Commercial TE devices are rigid, consisting of n- and p-type TEs connected electrically in-series and in-parallel through metallic interconnects. The rigidity of these conventional devices[5,6] limits applications.

Flexible TE sheets and nonwoven fabrics based on poly(styrenesulfonate)-doped poly(3,4-ethylenedioxythiophene),[7–9] doped carbon nanotube sheets,[10,11] and graphite composites[12] have been demonstrated in recent pioneering work. However, these sheet-based devices harvest thermal energy in the in-plane direction, rather than in more desirable sheet-thickness direction. TE textiles based on metal wires or metal wire sheaths have been used to harvest thermal energy in the textile thickness directions, but the extremely low figure of merit (ZT) of the metals limited their performance.[13,14] In other work, which resulted in a high ZT for thickness-direction thermal-energy harvesting, Kim et al.[15] screen printed Sb_2Te_3 and Bi_2Te_3 pellets on a bendable glass textile and incorporated this structure into flexible rubber sheets. Though a textile was not fabricated, Liang et al.[16] have used a mat of PbTe-coated glass fibers for a single-leg energy harvester that was wrapped on a hot pipe to harvest thermal energy. Additionally, concepts for novel TE textiles that harvest thermal energy in the through-thickness textile direction have been proposed in patents, but neither fabrication methods nor performance results on fabricated textiles were provided.[17,18]

We here describe the fabrication of flexible, woven, and knitted textiles based on electrospun polymer nanofiber cores that are coated with n- and p-type semiconductor sheaths (Bi_2Te_3 and Sb_2Te_3, respectively) and twisted into flexible yarns. Our work focuses on the most practical case, where the thermal gradient is in the textile thickness direction, instead of the in-plane direction.[10,11] TE textiles were fabricated by knitting or weaving n- and p-type TE yarns into patterns that electrically connect segments of these yarns in series and in parallel. Alternatively, yarns containing alternating n- and p-type segments (linked by metallic interconnects) are woven in one direction and separated by insulating yarns. These textile designs, suitable for through-thickness TE power generation, contain n- and p-type regions that alternate in the textile thickness direction, like in conventional TE arrays.

Textile structures were fabricated by combining separate n- and p-type yarns into woven or knitted structures or by weaving yarns containing alternating n- and p-type segments, which we call tiger yarns (**Figure 1**). Separately prepared n- and p-type TE yarns were incorporated into textiles using zigzag- or garter-stitch weaves, as illustrated in Figure 1a,b. These textile structures provide electrical pathways between segments of the n- and p-type yarns, so that electrons and holes flow from the hot source to the cold source in these segments. The correspondence between these textile structures and the conventional TE structures is provided in Figure 1d,e.

The textile structure produced by the zigzag stitch, shown in Figure 1a, has been previously demonstrated using chromel/alumel thermocouple wires,[14] but the realized power generation was extremely low (0.166 μW per couple). This zigzag structure is easily fabricated, but requires insulating yarns in both the orthogonal yarn directions to separate hot and cold sources, which reduces the density of TE couples. The main advantage of the garter-stitch (Figure 1b) knitted structure is that no insulating yarns are needed, since the yarn loops in the textile automatically alternate between the top and bottom surfaces. While this structure does not need insulating yarns to separate hot and cold side junctions, we utilize insulating yarns to enable better control of junction location during hand weaving. Both zigzag-stitch and garter-stitch textiles can be easily upscaled using fabrication technologies commonly used in the textile industry. The tiger-yarn textile structure, which is a plain weave of identical segmented TE yarns, which contain alternating n- and p-type segments, is shown in Figure 1c. This structure, which is quite similar to that used for commercial TE generators, has been proposed by Shtein and co-workers,[13,17]

Dr. J. A. Lee, Dr. A. E. Aliev, Dr. J. S. Bykova, Dr. M. Jung de Andrade, Dr. X. Lepró, Prof. A. A. Zakhidov, Dr. S. Roth, Prof. R. H. Baughman
The Alan G. MacDiarmid NanoTech Institute
The University of Texas at Dallas
Richardson, TX 75080, USA
E-mail: ray.baughman@utdallas.edu
Dr. J. A. Lee, H. J. Sim, Prof. S. J. Kim
Center for Self-powered Actuation and Department of Biomedical Engineering
Hanyang University
Seoul 133-791, South Korea
E-mail: sjk@hanyang.ac.kr
Dr. J. S. Bykova
Nano-Science and Technology Center
Lintec of America
Richardson, TX 75080, USA
Dr. D. Kim, Prof. J.-B. Lee
Department of Electrical Engineering
The University of Texas at Dallas
Richardson, TX 75080, USA
Prof. G. M. Spinks
ARC Centre of Excellence for Electromaterials Science
Intelligent Polymer Research Institute
University of Wollongong
Wollongong, New South Wales 2522, Australia

DOI: 10.1002/adma.201600709

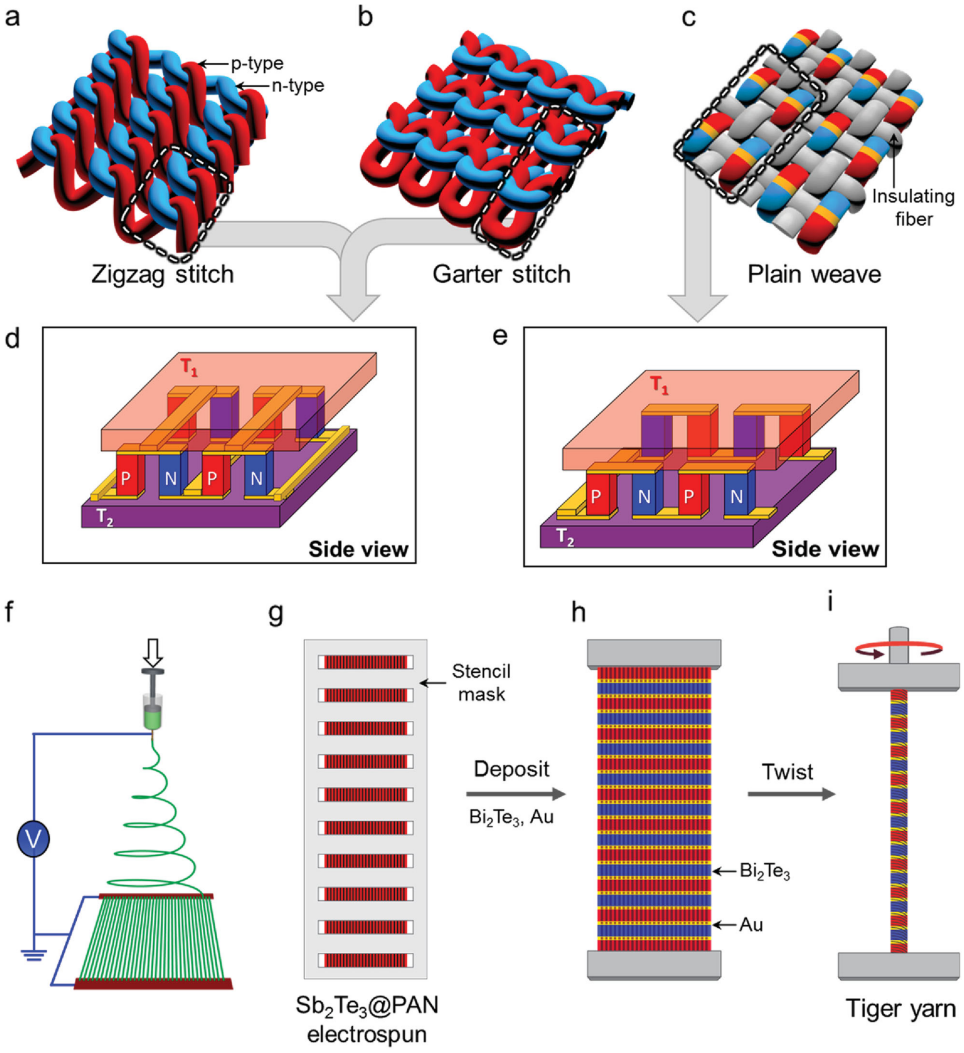

Figure 1. TE yarns and textiles and their fabrication. a–c) Illustration of TE textiles utilizing a zigzag stitch, a garter stitch, and a plain weave, respectively. Red and blue yarns and yarn segments contain polymer nanofibers that are over coated with n-type and p-type TEs, respectively. In (c), n and p nanofiber segments are separated by gold-coated segments (yellow) and the grey yarns are insulating. d) Illustration of the series–parallel electrical connectivity of TE elements for the highlighted areas of (a) and (b). e) Illustration of the series electrical connectivity of TE elements for the highlighted area of (c). The yellow bars in (d) and (e) are electrical interconnects between the pictured n and p TE element. f) Illustration of the electrospinning process used to make PAN nanofiber sheets for conversion into a yarn. A PAN solution in the syringe is extruded through the metal needle. A high voltage supply is connected to the spinning tip and to two counter electrodes, so that highly aligned PAN nanofiber sheets are collected. g,h) Illustration of the stencil-mask-based method used to provide alternating p-Au-n segments for tiger yarns by sequentially sputtering Sb_2Te_3-gold-Bi_2Te_3 on both sides of a PAN nanofiber sheet. i) Illustration of the twist spinning process used to convert the nanofiber sheet into a tiger yarn.

who made a tiger-type fiber by evaporating silver and nickel segments on a silica fiber. To increase the generated voltage, we used a single tiger yarn to provide in-series connected TE segments, rather than the combination of in-series and in-parallel connected TE segments of the zigzag- and garter-stitch textiles. When woven using conventional textile manufacturing processes, the TE tiger yarns would be in the weft direction, which is the direction in which yarns are inserted into a parallel array of other fibers (called the warp fibers). Hence, the weft direction fibers go above and below the warp fibers to form the textile. Insulating fibers were included in the weft direction to avoid the shorting of adjacent yarn segments, and in the warp direction to increase the separation between hot and cold junctions. Gold-coated yarn segments separated n- and p-type-coated segments, so that improved electrical interconnection was obtained between n- and p-segments and improved thermal contact was obtained with cold and hot sources.

Separate n-type and p-type yarns were prepared by depositing Bi_2Te_3 and Sb_2Te_3, respectively (Figure S1, Supporting Information). Highly aligned sheets of polyacrylonitrile (PAN) nanofibers, with average nanofiber diameter of ≈600 nm, were electrospun on two parallel wire collectors (Figure 1f). Semicrystalline TE films (100–110 nm thick) were next deposited on both sides of the sheet substrate to produce sheath-core nanofiber structures containing ≈50% by volume of active material. Twist insertion into the sheets, followed by a thermal annealing at 200 °C to crystallize the semiconductors, results in a strong, flexible sheath–core TE

yarns. Depending upon only the thickness of PAN sheets, since the nanofiber diameter and sheet width (≈1.2 cm) were kept constant, the resulting yarn diameter ranged from 300 to 380 μm and the yarn cross-section contained ≈18 000 TE nanofibers. These highly porous yarns are resistant to mechanical damage, which enables them to be knitted and woven into textiles without producing significant change in electrical resistances or thermopowers. As an example of yarn robustness, the electrical resistance of the Bi_2Te_3 yarn undergoes little change during stretching up to yarn failure at ≈10.5% strain, where the density-normalized stress is 2.5 MPa cm^3 g^{-1} (Figure S2, Supporting Information). This mechanical robustness is further indicated for the nonsegmented Sb_2Te_3 yarn by the observation that the yarn's electrical resistance increased by only ≈0.9% after 100 cycles of repeated bending on a mandrel to a curvature of 3.1 cm^{-1} (Figure S3, Supporting Information). The likely reason for a small resistance decrease during bending is that this severe bending of the yarn increases the yarn density, thereby decreasing yarn resistance by increasing electronic interconnections between nanofibers.

The advantage of the present TE textiles is that they are true TE textile containing TE yarns, rather than TE elements printed on a glass fabric, as in previous work.[15] This advantage is evidenced by the absence of a significant electrical resistance change (below ≈0.2%) when the zigzag-stitch textile was bent around a 0.5 mm radius mandrel. In contrast, the smallest bending radius that was characterized for TE disks printed on commercially available glass fabric was 20 mm.[15]

Tiger yarns were fabricated by first sputtering alternating strips of Sb_2Te_3 and Bi_2Te_3 (Figure 1g–i) on both sides of the electrospun PAN nanofiber sheet using a stencil mask, and then interconnecting these TE strips using narrow sputtered gold strips (see details in Figure S4, Supporting Information). The thicknesses of these coatings were 110 nm for the TEs and 75 nm for the gold. The thereby-coated nanofiber sheets were then twisted into yarns using an electric motor, typically using a twist density of ≈630 turns per meter, relative to the initial sheet length (Figure 1i).

Figure 2a,b demonstrates that the initial tiger structure is retained during twist insertion and subsequent complete yarn untwist. The X-ray diffraction patterns (see Figure S5, Supporting Information) indicate that the Bi_2Te_3 and Sb_2Te_3 are in their trigonal crystalline phases[19,20] (space group *R*-3m) after annealing, with grain size up to 20 nm. The scanning electron microscopy (SEM) images of the Bi_2Te_3 and Sb_2Te_3 yarns, shown in Figure 2c,d, indicate nearly parallel nanofiber alignment and a relatively narrow distribution of coated fiber diameters (600 ± 100 nm). As shown in the SEM images (Figure 2e,f), the Sb_2Te_3 yarn has a highly porous structure, which is also the case for the Bi_2Te_3 yarn. Thermal gravimetric analysis of pure electrospun PAN (Figure S6, Supporting Information) shows an initial loss of absorbed water (between 95 and 130 °C) and fiber pyrolysis[21] at 300 °C. The temperature onset for weight loss due to pyrolysis was significantly shifted to ≈400 °C when the electrospun PAN was coated with TEs, indicating that the TE sheath is providing protection for the polymer nanofiber core.

The schematic drawings of **Figure 3**a–c provide more structural detail for the textile topologies used to harvest electrical energy from a through-thickness thermal gradient. Two of the textile designs shown in Figure 3a,b include parallel and series electrical connections formed at the junctions between n- and p-type yarns (which are indirect, through a separating conductor). The total generated power depends on the number of n–p couples, while the voltage and current output depends upon the interconnection of these couples. The tiger-yarn,

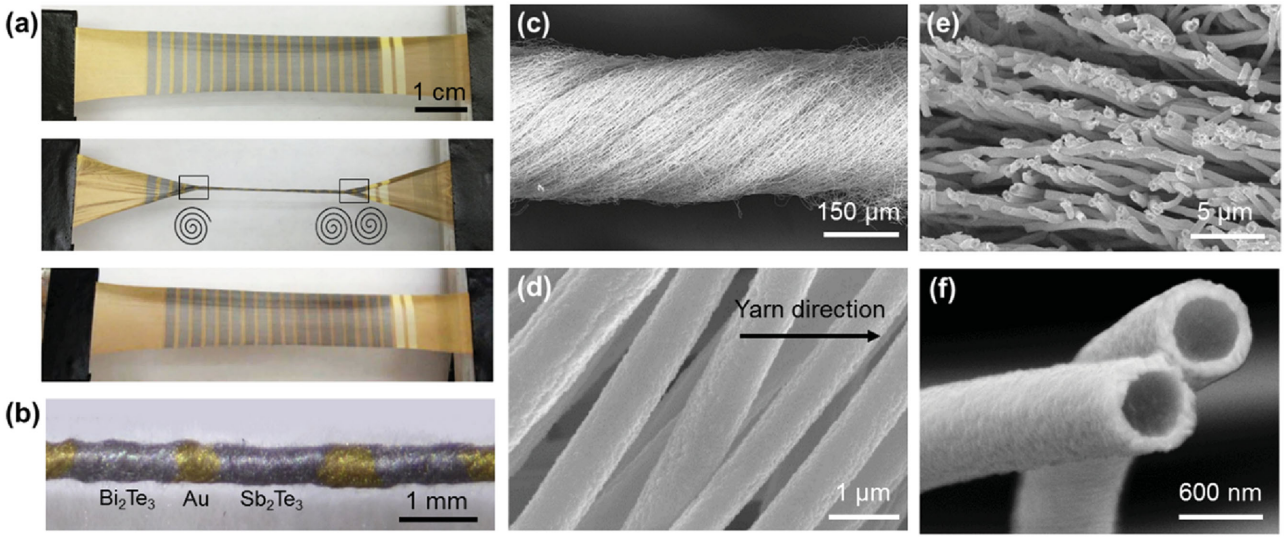

Figure 2. Retention of the tiger structure during twist-based yarn fabrication and images of Sb_2Te_3/PAN yarn. a) Photographs showing retention of the initial tiger structure (top image) during twist insertion (middle image) and during complete yarn untwist (bottom image). The tiger structure results from strips of $(Au/Sb_2Te_3/Au/Bi_2Te_3)_n$ that are initially orthogonal to the sheet length. These images are from Movie S1 (Supporting Information). b) Optical image showing the $(Au/Bi_2Te_3/Au/Sb_2Te_3)_n$ structure of the tiger yarn. c–f) SEM images showing lateral (c,d) and cross-sectional (e,f) images of a Sb_2Te_3/PAN yarn. The cross-sectional SEM images show a highly porous yarn structure that retains the layer structure of the original sheet. The cross-sectional image of (f) shows that the diameter of the Sb_2Te_3-coated nanofiber is ≈600 nm and that the Sb_2Te_3 coating is ≈110 nm thick.

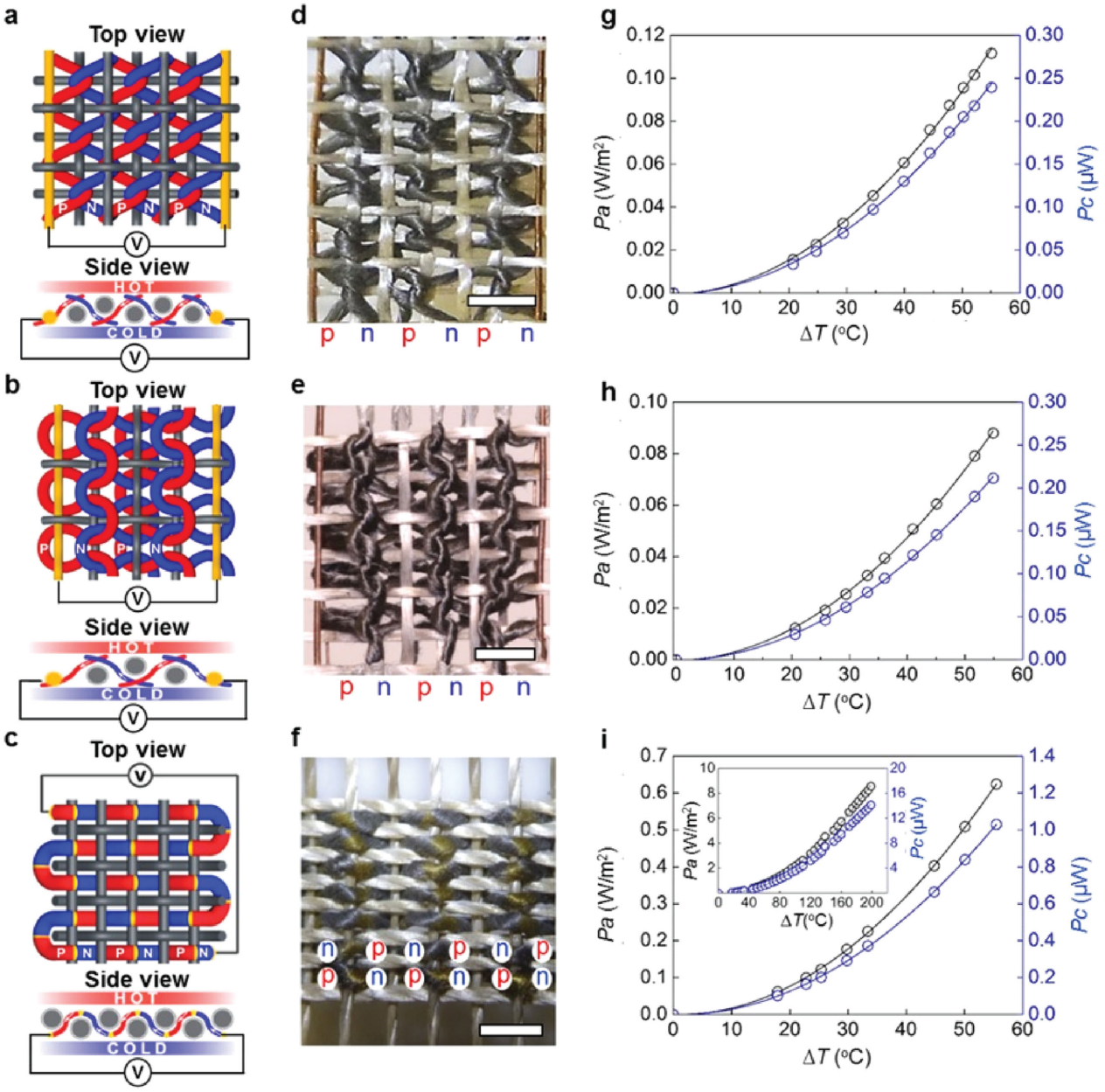

Figure 3. Structure and performance of TE textiles. a–f) Schematic illustrations (a–c) and photographs (d–f) of realized zigzag-stitch, garter-stitch, and plain-weave TE textiles, respectively. The scale bars are 2 mm long. g–i) The output power per textile area and per TE couple, measured as a function of the temperature difference (ΔT) for zigzag-stitch, garter-stitch, and plain-weave TE textiles, respectively. The inset of (i) shows the output power of a plain-weave TE textile for a ΔT of up to 200 °C.

plain-weave textile of Figure 3c, requires correct placement of n-type and p-type segments, since the pitch of the weave must be aligned to match the segment length, so that successive n–p junctions alternate between hot and cold surfaces. However, since the TE textiles must be thick in order to maximize the temperature drop across the textile (presently about 1.3 mm thick for the tiger-yarn TE textile), the n-type and p-type yarn segments in the tiger yarn are fairly long. Hence, high accuracy in positioning these segments is not required. For all textiles, the thermally generated electrical output was collected by thin copper wires that were woven into the warp direction along two edges of the textile, thereby connecting the parallel arrays of in-series connected multicouples. Photographs of the fabricated TE textiles are shown in Figure 3d–f and Figure S7 (Supporting Information).

Energy-harvesting measurements, to obtain maximum power output by resistance matching, were performed in air using the home-built thermal-gradient system illustrated in Figure S8 (Supporting Information). The electrical power outputs generated by the three textile structures, normalized to

the surface areas and to the number of couples, are shown in Figure 3g–i, respectively. The generated power quadratically increased with the temperature gradient, ΔT, applied across the textile thickness as $P_a \approx \sigma S^2(\Delta T)^2$, where σ is the electrical conductivity and S is the Seebeck coefficient. Also, the results of Figure S9 (Supporting Information) show that the textile can be upscaled without loss of power output per couple. Using ΔT = 55 °C, the tiger-yarn plain-weave textile provided a substantially higher output power (per area and per couple, ≈0.62 W m^{-2} and ≈1.01 µW, respectively) than for the textiles made by knitting individual n- and p-type TE yarns (0.11 W m^{-2} and 0.24 µW for the zigzag-stitch textile, and 0.09 W m^{-2} and 0.21 µW for the garter-stitch textile). Increasing ΔT to ≈200 °C (see inset of Figure 3i) dramatically increased the generated power per area (8.56 W m^{-2}) and per couple (14.1 µW), in accordance with the expected dependence of electrical power on $(\Delta T)^2$. The higher per junction power output (at given ΔT) for the tiger-yarn textile, compared with that for the other textiles, reflects the 1.8 times higher per-couple resistances for the zigzag-stitch textile and garter-stitch textile than for the plain-weave textiles. This higher resistance results from the longer leg length for the zigzag-stitch (≈2.3 mm) and garter-stitch (≈2.3 mm) textiles than for plain-weave textile (1.5 mm).

Since previously reported textiles comprising TE fibers used metals that have very low Seebeck coefficients, the generated electrical power per area was minute compared with the presently realized 8.56 W m^{-2} for ΔT = 200 °C and 0.52 W m^{-2} for ΔT = 50 °C. By screen printing 12.7 mm diameter, 0.5 mm thick pellets of Bi_2Te_3 and Sb_2Te_3 on a glass fabric, and subsequent annealing at above 500 °C, Cho and co-workers reported a much higher electric power per area for ΔT = 50 °C (38 W m^{-2}),[15] but the TE elements in this structure are neither very flexible nor yarn based. Using flexible sheets of n-doped and p-doped carbon nanotubes, the Roth/Carroll team[10] obtained (for an in-plain temperature gradient of 50 °C) an electrical power output per couple of 3.8 nW, which is much lower than for our plain-weave tiger-yarn textile (0.84 µW per couple for a ΔT of 50 °C in the textile thickness direction). Using carbon nanotube sheets and a similar approach, Yu and co-workers obtained an electrical power output of ≈25 nW per couple for ΔT = 32 °C.[11] For comparison, the tiger-yarn TE textile generates 13 times higher power per couple (≈334 nW for ΔT = 32 °C).

The presently reported areal power densities of plain-weave textiles can be dramatically increased, as discussed in the Supporting Information file. The first strategy is to increase by a factor of 5.2 the fraction of the TE yarn volume that is occupied by the TE fibers, from the present 10% to the 52% that we have recently demonstrated for analogous sheath–core TE fibers based on electrospun Kevlar. The second strategy is to increase the fraction of the TE textile that is occupied by the TE yarn. This filling factor is highest for the tiger-yarn-based plain-weave textile, and can be increased by at least a factor of 3.4 by decreasing the diameter of insulating yarns and by operating a fraction of the TE yarns in parallel, so that the number of insulating yarns can be reduced. Additionally, the electrical conductivity of the Bi_2Te_3 part of the n–p couple is six times lower than can be obtained for optimized Bi_2Te_3. Consequently, we predict that it is possible to increase the output areal power density from the presently measured 8.6 W m^{-2} for a ΔT = 200 °C to $5.2 \times 3.4 \times 6.0 \times 8.6$ W m^{-2} = 929 W m^{-2}. For comparison, areal power densities of 3567 and 4250 W m^{-2} have been reported for state-of-art,[22–24] completely rigid commercial TEs, based on the Bi_2Te_3/Sb_2Te_3 couple, when operated at hot plate to cold plate temperature differences of 200 and 180 °C, respectively.

Table 1. Properties of single nanofibers, nanofiber sheets, and twisted nanofiber yarns. The thermal conductivities (λ) and electrical conductivities (σ) are normalized with respect to the amount of TE. The Seebeck coefficient is S and ZT is the TE figure of merit.

	Sb_2Te_3/PAN (p-type)			Bi_2Te_3/PAN (n-type)		
	Nanofiber	Sheet	Yarn	Nanofiber	Sheet	Yarn
λ [W m^{-1} K^{-1}]	4	2.9	3	3	2.3	1.2
σ [10^4 S m^{-1}]	10	6.07	7.5	2.2	2.03	0.88
S [µV K^{-1}]	255	160	178	–250	–141	–176
ZT	0.48	0.16	0.24	0.14	0.05	0.07

The open-circuit voltages and short-circuit currents for each textile are shown in Figure S10–S12 (Supporting Information). A temperature difference of ΔT = 55 °C across the textile provides open-circuit voltages per couple of 15.8, 14.8, and 11.9 mV for the zigzag-stitch, garter-stitch, and plain-weave textiles, respectively. These voltages are lower (19.5 mV) than calculated from the measured Seebeck coefficients of n- and p-yarns (178 and –176 µV K^{-1}, respectively, **Table 1**), which might result from the thermal shorting of temperature gradients in the textile by the supporting structure of electrically insulating yarns.

It is important to note that the temperature drop across the TE couples was a large fraction of the difference in hot and cold source temperature even when the textiles were only about 1 mm thick. Specifically, the percent temperature drop (relative to the temperature difference between hot and cold plates) varies for the plain-weave textile from 68.5% (for a hot plate temperature of 79 °C) to 84% (for a hot-plate temperature of 177 °C). By increasing the diameter of the insulating yarn in the warp direction relative to the TE weft yarn, these percentages can be further increased as a result of the corresponding increase in textile thickness. Furthermore, the detailed results (provided in Figure S13, Supporting Information) show that we can already obtain a temperature drop of up to 160 °C for 1.5 mm-thick plain-weave textile.

While high temperatures could not be used for the zigzag- and garter-stitch textiles, because of degradation of the silver-paste electrical contacts, we were able to evaluate these temperatures for the plain-weave textile, which used gold contacts. An open-circuit voltage per couple of 45.2 mV was obtained for the plain-weave structure at ΔT = 200 °C, which corresponds to an average Seebeck coefficient magnitude per leg for this temperature range of 113 µV K^{-1}. As expected,[25] because the Seebeck coefficients for these TEs decrease with increasing temperature, this high-temperature Seebeck coefficient is lower than the values for each leg at room temperature, which are reported in Table 1. Figure S14 (Supporting Information) shows that a yarn couple between separate n-type and p-type yarns can be operated up to ΔT = 200 °C, if a mechanical load is used (instead of silver paste) to decrease the resistivity of the interconnection between these yarns. However, the presented

results on power output per couple show that mechanical interconnection is insufficient to reduce the interconnect resistance to acceptable values.

The short-circuit currents per couple at $\Delta T = 55$ °C for the zigzag-stitch, garter-stitch, and plain-weave textiles, were 0.061, 0.057, and 0.34 mA, respectively. This much higher current for the plain-weave textile (which uses gold contacts) than for the other textiles (which use silver-paste contacts) reflects the high resistance of the latter contacts. The generated power per area linearly increased with increasing $(\Delta T)^2$, as shown in Figure S10d, S11d, and S12d (Supporting Information), with slopes of 3.6×10^{-6}, 3.0×10^{-6}, and 2.3×10^{-5} mW cm^{-2} K^{-2} for the zigzag-stitch, garter-stitch, and plain-weave textiles, respectively.

In order to understand the performance obtained for the TE textiles, the observed properties of the individual nanofibers, the TE yarns, and the precursor nanofiber sheets can be compared with those for the textiles. As shown in Table 1, the nanofibers provided Seebeck coefficients ($S_{Bi2Te3} = -250$ μV K^{-1}, $S_{Sb2Te3} = 255$ μV K^{-1}), which are close to the highest values reported in literature ($S_{Bi2Te3} = -250$ μV K^{-1}, $S_{Sb2Te3} = 230$ μV K^{-1}).[26,27] While the electrical conductivity of the Sb_2Te_3 coating on individual nanofibers (10×10^4 S m^{-1}) was close to that previously reported for polycrystalline, nanostructured Sb_2Te_3 (from 5.5×10^4 to 9.0×10^4 S m^{-1}),[28] the Bi_2Te_3 coating had a lower conductivity (2.2×10^4 S m^{-1}) than previously realized for nanocrystals (5.6×10^4 S m^{-1}).[29] This problem with optimizing the electrical conductivity of Bi_2Te_3, which results from surface oxidation, is well known.[30]

In contrast, the thermal conductivities of the TE layers of the single nanofibers were higher than reported for bulk films of Bi_2Te_3 and Sb_2Te_3 (2.8 and 0.8 W m^{-1} K^{-1}, respectively)[28,31] but close to the thermal conductivity of single crystals (≈5 W m^{-1} K^{-1} for Sb_2Te_3).[32] Since the thermal conductivity of uncoated PAN nanofibers is very low, ≈0.03 W m^{-1} K^{-1},[33] compared to that for the Bi_2Te_3 and Sb_2Te_3, the thermal conductivity contribution of the fiber core can be ignored.

For comparison with the above results for the TE sheaths of single nanofibers, we now consider the thermal and electrical conductivities of twisted fibers and precursor nanofiber sheets, normalized with respect to the cross-sectional area of the TE component. With this normalization, the electrical and thermal conductivities based on TE components are quite similar for the nanofibers, nanofiber sheets, and nanofiber yarns. Without this correction for porosity and inactive components, the thermal and electrical conductivities of the yarns are reduced by a factor of 10 for porosity and an additional factor of 2 for inactive components. The corresponding uncorrected thermal conductivities and electrical conductivities for the yarns, based on total cross-sectional area, are 0.3 ± 0.04 W m^{-1} K^{-1} and 6.8×10^3 S m^{-1} for Sb_2Te_3 and 0.12 ± 0.04 W m^{-1} K^{-1} and 0.8×10^3 S m^{-1} for Bi_2Te_3.

We have demonstrated the first examples of flexible textiles that utilize yarns comprising high-performance TEs. While it is easier to design textiles that harvest thermal gradients within the textile plane, we have used three different textile designs to demonstrate the more practically useful thermal-energy harvesting in the textile thickness direction. An output power of up to 8.56 W m^{-2} was obtained for a temperature difference of 200 °C in the textile thickness direction. In this initial work using nanofibers of high-performance TEs, various opportunities are described for dramatically improving textile performance by increasing the density of TE couples and TE yarns, improving electrical contacts, and increasing the electrical conductivity of one of the TEs (Bi_2Te_3 yarn). Using the presently obtained results, future improvements in TE performance and thermal stability of the core fiber could result in efficient energy-harvesting textiles that can be wrapped around a car's exhaust pipe or hot waste-stream pipes that exit chemical or power plants. Since various other TEs can be deposited on core nanofibers, the present work could be extended to higher temperature textiles that use thermoelectrics like PbTe and SiGe. For application at extreme temperatures, the present core polymer nanofibers can be replaced by inorganic fibers as long as the nanofiber diameter is sufficiently small to provide the needed mechanical robustness during twist insertion.

Experimental Section

PAN Electrospinning: Using a method similar to those previous described,[34] nanofibers were electrospun from a 10 wt% solution of PAN in *N*,*N*-dimethylacetamide (DMAC). A syringe pump (KDS 100, KD Scientific) fed this solution into a 5 mL plastic syringe (Kovax-syringe 5 mL, 22GX 11/4″, Korea Vaccine Co., LTD) that contained a 22 gauge stainless-steel needle. The solution feed rate was 20 μL min^{-1} and the distance between the needle tip and the parallel metal collectors, which are orthogonal to the syringe needle, was ≈13 cm. The distance between the parallel metal collectors in Figure 1f was 8 cm. During the spinning process, which resulted in sheet of parallel nanofibers, a high-voltage supply (MHP40-02A, model IHPS 40 kV, 2 mA, Wookyung Tech) provided a 24 kV potential of the spinning tip relative to the metal collectors. Figure 1f shows a schematic image of the two electrodes and a collected parallel array of nanofibers. The existence of these two metal collector electrodes, which are counter electrodes to the spinning electrode, causes the charged spun nanofibers to align as a parallel array.

Deposition of TEs on Electrospun PAN Nanofiber Sheets: High-purity Bi_2Te_3 and Sb_2Te_3 disk targets (Kurt J. Lesker Company) were used for radio-frequency (RF)-magnetron sputtering, using a DC/RF Reactive Magnetron Sputter (AJA International, Inc.). Sputtering was performed at 100 W using an Ar flow of 12 sccm and a chamber pressure of below 1×10^{-5} Pa. Uniform deposition of TE films were achieved by rotating the PAN substrate at 55 rpm during the sputtering process. These conditions provided deposition rates of between 0.32 and 0.35 nm s^{-1} for Bi_2Te_3 and between 0.3 and 0.38 nm s^{-1} for Sb_2Te_3. Using separate steps, the electrospun PAN sheets were coated on both sides with the TE. After this deposition, the area density of the n- or p-type sheets was ≈0.15 mg cm^{-2}. Figure S4 (Supporting Information) shows the patterning technique and the stencil mask used for the preparation of the segmented tiger yarns. For all investigated TE nanofibers, the fraction of the sheath-core nanofiber that was occupied by TE was ≈50%, and we found that maintaining approximately this fraction was important for enabling twist insertion, and subsequent yarn densification to form yarn.

Yarn Twist and Annealing: The above described sheets of TE-coated nanofibers were twisted into yarns as follows. One end of the sheet was attached to the shaft of an electric motor, while the other end was attached to a stationary flat panel. Movie S1 (Supporting Information) shows the spinning of a nanofiber sheet into yarn, which involves the formation of two spinning wedges at opposite sheet ends. The amount of inserted twist was ≈630 turns per meter, based on the initial sheet length. After twisting, the yarns were transferred to glass slides, fixed at both ends with Kapton tape, and annealed at 200 °C for 4 h in an Ar/H_2 (95/5 vol%) atmosphere in order to crystallize the TEs.

Supporting Information

Supporting Information is available from the Wiley Online Library or from the author.

Acknowledgements

This work was supported by the Creative Research Initiative Center for Self-powered Actuation and the Korea-US Air Force Cooperation Program Grant No. 2013K1A3A1A32035592 in Korea. Support at the University of Texas at Dallas was provided by Air Force Office of Scientific Research grants FA9550-15-1-0089 and AOARD-FA2386-13-4119, NASA grants NNX14CS09P and NNX15CS05C, and the Robert A. Welch Foundation grant AT-0029. Additional support was from the Australian Research Council and the Australian National Fabrication Facility.

Received: February 4, 2016
Revised: March 3, 2016
Published online: April 25, 2016

[1] P. Chen, T.-K. Chen, Y.-S. Wang, C.-C. Chen, *IEEE Sens. J.* **2009**, *9*, 1639.
[2] R. Ahiska, S. Dışlıtaş, *Gazi Univ J. Sci.* **2006**, *19*, 135.
[3] B. A. Cornell, V. L. B. Braach-Maksvytis, L. G. King, P. D. J. Osman, B. Raguse, L. Wieczorek, R. J. Pace, *Nature* **1997**, *387*, 580.
[4] Y. Zhao, A. Kumar, C. Hin, S. Priya, *Nanoscale Thermoelectrics, Lecture Notes in Nanoscale Science and Technology, Vol. 16*, Springer International Publishing Switzerland, Cham, Switzerland **2014**, p. 327.
[5] G. J. Snyder, E. S. Toberer, *Nat. Mater.* **2008**, *7*, 105.
[6] D. M. Rowe, *Thermoelectrics Handbook: Macro to Nano*, Taylor and Francis, CRC Press, New York, **2006**.
[7] T. Park, C. Park, B. Kim, H. Shin, E. Kim, *Energy Environ. Sci.* **2013**, *6*, 788.
[8] G.-H. Kim, L. Shao, K. Zhang, K. P. Pipe, *Nat. Mater.* **2013**, *12*, 719.
[9] A. M. Nardes, M. Kemerink, R. A. J. Janssen, J. A. M. Bastiaansen, N. M. M. Kiggen, B. M. W. Langeveld, A. J. J. M. V. Breemen, M. M. D. Kok, *Adv. Mater.* **2007**, *19*, 1196.
[10] C. A. Hewitt, A. B. Kaiser, S. Roth, M. Craps, R. Czerw, D. L. Carroll, *Nano Lett.* **2012**, *12*, 1307.
[11] S. L. Kim, K. Choi, A. Tazebay, C. Yu, *ACS Nano* **2014**, *8*, 2377.
[12] M. Piao, G. Kim, G. P. Kennedy, S. Roth, U. Dettlaff-Weglikowska, *Phys. Status Solidi B* **2013**, *250*, 2529.
[13] A. Yadav, K. P. Pipe, M. Shtein, *J. Power Sources* **2008**, *175*, 909.
[14] N. Yamamoto, H. Takai, *Elect. Eng. Jpn.* **2002**, *140*, 16.
[15] S. J. Kim, J. H. We, B. J. Cho, *Energy Environ. Sci.* **2014**, *7*, 1959.
[16] D. Liang, H. Yang, S. W. Finefrock, Y. Wu, *Nano Lett.* **2012**, *12*, 2140.
[17] M. Shtein, K. P. Pipe, *US 7970242 B2*, **2011**.
[18] M. Plissonnier, Y. Breton, I. Chartier, T. Lanier, C. Navone, *US 20090025774 A1*, **2009**.
[19] H.-J. Lin, K.-J. Kang, J.-D. Hwang, H.-S. Chu, H.-H. Huang, M.-C. Wang, *Metall. Mater. Trans. A.* **2013**, *44A*, 2339.
[20] P. Christian, P. O'Brien, *J. Mater. Chem.* **2005**, *15*, 4949.
[21] W. Zhang, Y. Wang, C. Sun, *J. Polym. Res.* **2007**, *14*, 467.
[22] K. T. Zorbas, E. Hatzikraniotis, K. M. Paraskevopoulos, in *Proc. 5th Eur. Conf. Thermoelectrics*, The European Thermoelectric Society **2007**.
[23] HT-9-3-25 thermoelectric cooler, http://www.knap.at/datenblaetter/pel/pel_mel_ht9-3-25.pdf; accessed: March, 2016.
[24] TEG2-07025HT-SS, http://tecteg.com/wp-content/uploads/2014/09/SpecTEG2-07025HT-SS.pdf; accessed: March, 2016.
[25] W. Liu, K. C. Lukas, K. McEnaney, S. Lee, Q. Zhang, C. P. Opeil, G. Chen, Z. Ren, *Energy Environ. Sci.* **2013**, *6*, 552.
[26] L. M. Goncalves, C. Couto, P. Alpuim, A. G. Rolo, F. Völklein, J. H. Correia, *Thin Solid Films* **2010**, *518*, 2816.
[27] W. J. Qiu, S. H. Yang, T. J. Zhu, J. Xie, X. B. Zhao, *J. Electron. Mater.* **2011**, *40*, 1506.
[28] M. Saleemi, A. Ruditskiy, M. S. Toprak, M. Stingaciu, M. Johnsson, I. Kretzschmar, A. Jacquot, M. Jägle, M. Muhammed, *J. Electron. Mater.* **2014**, *43*, 1927.
[29] Y. Zhao, J. S. Dyck, B. M. Hernandez, C. Burda, *J. Am. Chem. Soc.* **2010**, *132*, 4982.
[30] H. Bando, K. Koizumi, Y. Oikawa, K. Daikohara, V. A. Kulbachinskii, H. Ozaki, *J. Phys.: Condens. Matter* **2000**, *12*, 5607.
[31] U. Pelz, K. Kaspar, S. Schmidt, M. Dold, M. Jägle, A. Pfaadt, H. Hillebrecht, *J. Electron. Mater.* **2012**, *41*, 1851.
[32] Č. Drašar, M. Steinhart, P. Lošťák, H.-K. Shin, J. S. Dyck, C. Uher, *J. Solid State Chem.* **2005**, *178*, 1301.
[33] N. Sabetzadeh, H. Bahrambeygi, A. Rabbi, K. Nasouri, *Micro Nano Lett.* **2012**, *7*, 662.
[34] R. Jalili, M. Morshed, S. Abdolkarim, H. Ravandi, *J. Appl. Polym. Sci.* **2006**, *101*, 4350.